This is the accepted manuscript made available via CHORUS. The article has been published as:

Verifying a quasiclassical spin model of perturbed quantum rewinding in a Fermi gas

J. Huang, Camen A. Royse, I. Arakelyan, and J. E. Thomas

Phys. Rev. A **108**, L041304 — Published 20 October 2023

DOI: 10.1103/PhysRevA.108.L041304

Verifying a quasi-classical spin model of perturbed quantum rewinding in a Fermi gas

J. Huang, Camen A. Royse, I. Arakelyan, and J. E. Thomas
[1] *Department of Physics, North Carolina State University, Raleigh, NC 27695, USA*
(Dated: August 30, 2023)

We systematically test a quasi-classical spin model of a large spin-lattice in energy space, with a tunable, reversible Hamiltonian and effective long-range interactions. The system is simulated by a weakly interacting Fermi gas undergoing perturbed quantum rewinding using radio-frequency(RF) pulses. With single-shot analysis techniques, the measurement of energy-resolved spin density quantitatively substantiates the classical treatment of this many-body spin system. This work also elucidates the effects of RF detunings on the system and measurements, pointing the way to new correlation measurement methods.

Measurement of coherence, entanglement, and correlations in time-reversible many-body spin lattices is of great interest, broadly impacting our understanding of quantum measurement and information processing [1–3]. A nearly ideal platform for exploring large spin-lattices is a weakly interacting Fermi gas, containing $N \simeq 10^5$ atoms that simulates a tunable, reversible, collective Heisenberg Hamiltonian, which is a paradigm for quantum magnetism [4]. The trapped cloud behaves as a spin lattice in energy-space with effective long-range interactions [2, 5–14]. Remarkably classical hydrodynamic behavior has been observed in large spin materials with long range interactions and disorder [15]. However, it is unclear if a weakly interacting Fermi gas obeys classical spin evolution [16–19].

Spin waves observed in nearly collisionless Fermi gases have been explained by several models [6–11, 13], including a 1D quasi-classical spin evolution model [8], which appeared to fail in perturbed quantum rewinding experiments [20]. In such experiments, an RF pulse rotates the entire spin system by an angle ϕ_x about the x-axis as a perturbation in between forward and backward evolution. In a quantum picture, the ϕ_x rotation changes the relative phases of the superposed total angular momentum states that describe the system, i.e., $|S, M_x\rangle \rightarrow e^{-iM_x\phi_x}|S, M_x\rangle$ for each state, leading to coherence amplitudes with ϕ_x-dependent phases between states differing in M_x. To fit the data, an unphysical scattering amplitude $\approx$ 2.5 times the measured value was needed [20], questioning the adequacy of the quasi-classical treatment and suggesting possible quantum effects.

In this work, we report precise, systematic tests of a quasi-classical spin model using single-shot measurements of the spin density profiles from perturbed quantum rewinding experiments. Such experiments are ideal for testing the model, since unperturbed rewinding experiments can be implemented in advance to prove that the system is reversed properly without model-dependent fits, as shown in Fig. 1. We show the advantages of single-shot data analysis for studies of ensemble-averaged energy-resolved spin density, and quantitatively demonstrate the important roles of different RF detunings during the forward and backward evolution periods. By using two detunings as separate fit parameters, the data is explained by the model using the measured scattering length. The new approach reported here validates the modified quasi-classical treatment of this quantum spin system and suggests detuning-independent measurement methods for future correlation studies, avoiding probabilistic methods in data selection [12].

Our experiments [21], employ degenerate clouds of ^{6}Li containing a total of $N = 6.5 \times 10^4$ atoms initially in a single spin state. The cloud is confined in a harmonic, cigar-shaped optical trap, with oscillation frequencies $\omega_x/2\pi = 24.4$ Hz in the axial direction and $\omega_r/2\pi = 650$ Hz in the radial direction. The corresponding Fermi temperature $T_F = 0.73\,\mu$K and $T/T_F = 0.31$. RF pulses prepare coherent superpositions of the two lowest hyperfine-Zeeman states, which are denoted by $|1\rangle \equiv |\uparrow_z\rangle$ and $|2\rangle \equiv |\downarrow_z\rangle$. The experiments are done in the weakly interacting regime, where the energy-state changing collision rate is negligible over the time scale of the measurements [8].

As the single particle energies are *fixed* and the energy distribution is time independent [8], we approximate the cigar-shaped weakly interacting Fermi gas as a one-dimensional (1D) spin "lattice" in energy space [8], with a Hamiltonian

$$\frac{H(a)}{\hbar} = a\sum_{i,j\neq i} g_{ij}\,\vec{s}_i\cdot\vec{s}_j + \sum_i \Omega' E_i\, s_{zi} + \Delta(t) S_z. \quad (1)$$

We associate a "site" i with the energy $E_i = (n_i + 1/2)\,h\nu_x$ of the i$^{\text{th}}$ harmonic oscillator state along the cigar axis x. For each E_i, we define a dimensionless collective spin vector $\vec{s}(E_i) \equiv \vec{s}_i$.

The first term in Eq. 1 is the site-to-site interaction, proportional to the s-wave scattering length a and to the overlap of the harmonic oscillator probability densities for colliding atoms. In a WKB approximation, $g_{ij} \propto 1/\sqrt{|E_i - E_j|}$, which is an effective long-range interaction in the energy-space lattice [8]. For a zero temperature Fermi gas, the average interaction energy (in rad/s) is $a\bar{g} = 6.8\, n_0 \hbar a/m$, where n_0 is the peak density. For our experimental parameters, with $a = 5.2\, a_0$, $a\bar{g}/2\pi \simeq 2.0$ Hz.

The second term in Eq. 1 is an effective site-dependent Zeeman energy, arising from the quadratic spatial variation of the bias magnetic field along x, which produces

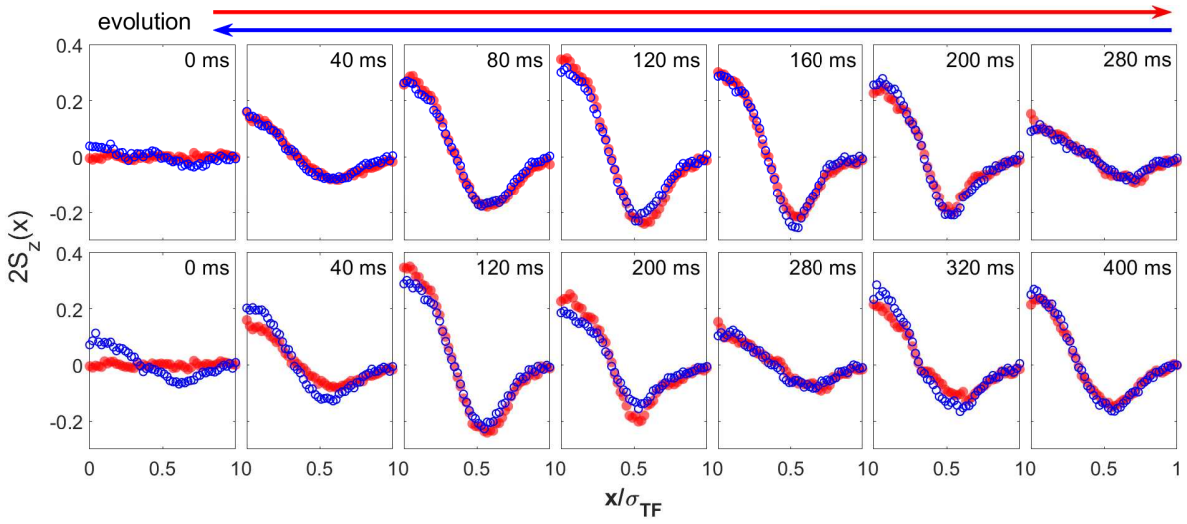

FIG. 1. Observing quantum rewinding by comparing the spin densities for forward evolution (red circles) and backward evolution (blue circles). The scattering length $a = 8.0\,a_0$ and $\sigma_{TF} \approx 335\,\mu$m. The Hamiltonian is reversed at $\tau_f = 280$ ms (top) and $\tau_f = 400$ ms (bottom). For forward evolution data, the time t_k shown on the top right corner of each tile is the total evolution time $t_{\rm fk}$: For the backward evolution data, the total evolution time $t_{\rm bk} = \tau_f + \tau_b$, where τ_f is the time at which reversal occurs, and $\tau_b = \tau_f - t_k$ is the backward evolution time, see Fig. 2. To avoid confusion with the x-axis of RF or Bloch frame, here, we clarify that x in all spatial profiles means axial direction along the longitudinal axis of the cigar-shaped cloud.

a spin-dependent harmonic potential. As $\omega_r/\omega_x = 26.6$, the corresponding effect on the radial motion is negligible, enabling a 1D approximation, where atoms in different radial energy states at site i have the same Zeeman energy. In Eq. 1, $\Omega' = -\delta\omega_x/(\hbar\omega_x)$, with $\delta\omega_x/2\pi = 14.9$ mHz for our trap [8]. For the mean energy $\bar{E}_x \simeq k_B T_F/4$, $\Omega'\,\bar{E}_x/2\pi \simeq 2.0$ Hz.

The last term in Eq. 1 arises from the time-dependent global detuning $\Delta(t)$, which plays a central role in the analysis of the rewinding data. Here, $S_z = \sum_i s_{zi}$. Fluctuations in the bias magnetic field and magnetic tuning of the scattering length cause $\Delta(t)$ to change at 5 kHz/G for $|1\rangle$-$|2\rangle$ superposition states.

To implement perturbed quantum rewinding, we employ the pulse sequence shown in Fig. 2 [20]. The system is initially prepared in a pure z-polarized spin state, $|\psi_{0z}\rangle$. The first $(\pi/2)_y$ pulse (0.5 ms), defined to be about the y-axis, creates an x polarized state, $|\psi_{0x}\rangle$. Here, the y- and x-axes are defined in the rotating frame of the RF pulses (RF-frame). Then, the system is allowed to evolve forward for a time τ_f. A voltage-controlled change of the RF phase by $\pi/2$ permits rotation about the x-axis by an angle ϕ_x. Applying a $(\pi)_y$ pulse (1 ms) and magnetically tuning the scattering length from $a \to -a$ (10 ms) inverts the sign of Hamiltonian shown in Eq. 1, causing the system to evolve backward for a time τ_b [21]. As described below, we perform experiments both with and without the final $(\pi/2)_y$ pulse, after which the spatial profiles of the $|\uparrow_z\rangle$ and $|\downarrow_z\rangle$ states are measured by two resonant absorption imaging pulses, separated by 10 μs, to obtain the single-shot spin density $S_z(x) = [n_{\uparrow_z}(x) - n_{\downarrow_z}(x)]/2$. For each shot, $S_z(x)$ is normalized to the total central density $n(0) = n_{\uparrow_z}(0) + n_{\downarrow_z}(0)$ to minimize errors arising from shot-to-shot variation in the atom number and cloud width. All spatial profiles are folded about $x = 0$ and displayed for $0 \le x \le \sigma_{TF}$.

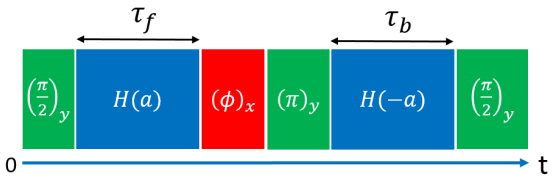

FIG. 2. Characterizing perturbed quantum rewinding. The atom cloud is initially prepared in a pure z-polarized spin state. The system runs forward for a time τ_f and backward for τ_b, after which the spatial profiles of the $|\uparrow_z\rangle$ and $|\downarrow_z\rangle$ states are measured. Green and red blocks represent RF pulses and rotation angles about the y- and x-axes respectively, whose durations are $<< \tau_f$, τ_b.

The reversibility of the system is tested using the pulse sequence of Fig. 2 with $\phi_x = 0$ and *without* the final $(\pi/2)_y$ pulse. This sequence measures the component of the collective spin vector $\vec{s}_i$ that was along the z-axis just prior to imaging. The longitudinal (z) component is insensitive to the detuning $\Delta(t)$ that causes a rotation of $\vec{s}_i$ about the z-axis relative to the RF-frame, enabling a robust test. In the data analysis, since $S_z = 0$ for $\phi_x = 0$, global spin balance is enforced to minimize the error from small shot-to-shot changes in the detuning of the RF pulses, which arises from magnetic field fluctuation.

In these experiments, it is essential to carefully calibrate the bias magnetic field B_0 at which the s-wave scattering length vanishes. This is best done by quantifying the reversal results using different magnetic fields, which is independent of fitting models and less sensitive to the initial conditions, in contrast to the method adopted in Ref. [8]. B_0 is found by minimizing the sum of the mean square differences between the forward and backward spin density profiles at corresponding times [21]. Unperturbed rewinding experiments done at scattering lengths of $\pm 5.2\,a_0$ and $\pm 8.0\,a_0$, suggest that $B_0 = 527.150(5)$ G, which is lower by 30 mG compared to the B_0 of Ref. [8].

Fig. 1 shows rewinding data (6-shot average) at corresponding forward(red) and backward(blue) evolution times for $a = 8.0\,a_0$ and $-8.0\,a_0$ respectively. With the calibrated B_0, the corresponding forward and backward spin density profiles demonstrate good agreement for reversal at 280 ms (top row), while reversal at 400 ms (bottom row) leads to greater differences between corresponding forward and backward data profiles.

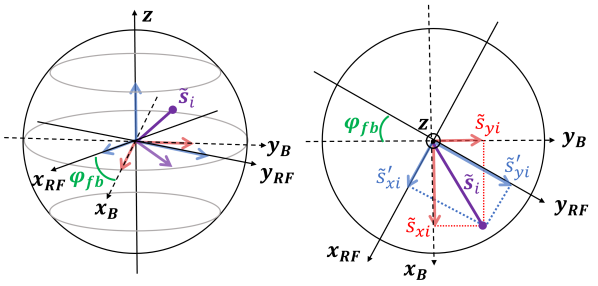

FIG. 3. Relation between the spin vector components in the radiofrequency(RF) and Bloch(B) frames for nonzero φ_{fb}.

Having established that the system is reversible for scattering lengths $|a| \leq 8.0\,a_0$ and evolution time $\tau \equiv \tau_f = \tau_b \leq 280$ ms, data are mainly obtained with $\tau = 200$ ms at $5.2\,a_0$ (denoted $[5.2\,a_0; 200\text{ ms}]$) using the full pulse sequence of Fig. 2. This provides stringent tests of quasi-classical collective spin vector models. Here, the final $(\pi/2)_y$ pulse is included to measure the transverse spin components that were along the x-axis in the RF frame in Fig. 3 just prior to imaging. For $\phi_x = 0$ and a detuning $\Delta(t)$ that is constant over the total sequence, the system is expected to rewind to the initial state, where the density profiles for both spins are Thomas-Fermi. For $\phi_x \neq 0$, however, the rewinding is perturbed, producing complex spin density profiles after the full sequence.

Fig. 4 shows single-shot spin density profiles for $\phi_x = \pi/2, \pi, 3\pi/2$. We obtain the corresponding energy-space profiles $s_{zi} \equiv s_z(E)$ by inverse Abel-transformation [22] of the spatial profiles, which is valid in a WKB approximation when energy space coherence is negligible and a quasi-continuum approximation is valid, as in our experiments [8].

To understand the perturbed rewinding data of Fig. 4, we include a time-dependent global detuning, $\Delta(t)$, in the Hamiltonian of Eq. 1. The detuning determines the relative angle between the RF-frame and the Bloch frame φ_{fb} in Fig. 3. Here, the RF frame is defined by x_{RF} and y_{RF} axes that rotate about the z-axis at the instantaneous RF frequency, $\omega_{RF}(t)$, tracking the *total* phase of the RF field. We define the rotation axes for all of the RF pulses in Fig. 2 to be in the RF frame, i.e., $x \equiv x_{RF}$ and $y \equiv y_{RF}$. The Bloch frame is defined by x_B and y_B axes that rotate at the instantaneous hyperfine resonance frequency $\omega_{HF}(t)$ for an atom of axial energy $E = 0$.

The detuning, $\Delta(t) = \omega_{HF}(t) - \omega_{RF}(t)$, causes the components of the spin vectors in the Bloch frame to rotate relative to the RF-frame by generally different angles $\varphi_f = \int_{\tau_f} dt\,\Delta(t)$ and $\varphi_b = \int_{\tau_b} dt\,\Delta(t)$, during the forward and backward evolution times, respectively, even for $\tau_b = \tau_f = \tau$ as in our experiments. Just after the forward evolution, the perturbing ϕ_x rotation is effectively applied about a rotated axis $\hat{e}_{x'} = \cos\varphi_f \hat{e}_x - \sin\varphi_f \hat{e}_y$ [21].

For each shot, the operator s_{zi} is measured for an ensemble of atoms in a selected energy group $E_i \in [E, E + \Delta E]$. The energy resolution ΔE of the inverse Abel-transform method is small enough that all of the atoms in the energy group evolve identically over the time scale of the pulse sequence. The measurements then yield the ensemble-average of the x-component relative to the RF frame just before the final $(\pi/2)_y$ pulse,

$$\tilde{s}'_{xi} = \cos\varphi_{fb}\,\tilde{s}_{xi} - \sin\varphi_{fb}\,\tilde{s}_{yi}, \tag{2}$$

where $\tilde{s}_{xi}$ aned $\tilde{s}_{yi}$ are the components in the Bloch frame [21], Fig. 3. For each measurement, the difference between the backward and forward phase shifts, $\varphi_f - \varphi_b \equiv \varphi_{fb}$, determines the relative contribution of the spin components in the Bloch frame to the measured projection in the RF frame.

To predict the measured s_{zi}, we employ a mean-field approximation to obtain a quasi-classical model [8], where the Heisenberg equations are solved numerically by treating the collective spin vectors as classical variables, which ignores quantum correlations between the spin vectors for different energy groups. The Heisenberg equations of motion for the collective spin vectors take a simple form in energy space, $\dot{\vec{s}}_i(t) = \vec{\omega}_i(t) \times \vec{s}_i(t)$, with

$$\vec{\omega}_i(t) = a \sum_{j \neq i} g_{ij}\,\vec{s}_j(t) + \Omega' E_i\,\hat{e}_z + \Delta(t)\hat{e}_z. \tag{3}$$

For a given choice of the forward and backward detunings, i.e., the phases φ_f and φ_b, s_{zi} is determined by numerical integration. An Abel transform of $s_{zi} \equiv s_z(E)$ then yields the corresponding spin density $s_z(x)$ [8].

Experimentally, 60 shots are taken for each set of parameters. Examples of single-shot data are shown in Fig. 4 and in the supplement [21]. Due to the complexity of the spatial profiles for $\phi_x \neq 0$, single-shot data analysis is essential for this experiment. Small variation ($\leq 5\%$) in cloud parameters results in shifted spatial profiles, even for fixed φ_f and φ_b, so averaging over shots with slightly different initial conditions can wash out the fine structure. Fig. 4 compares two quasi-classical models with

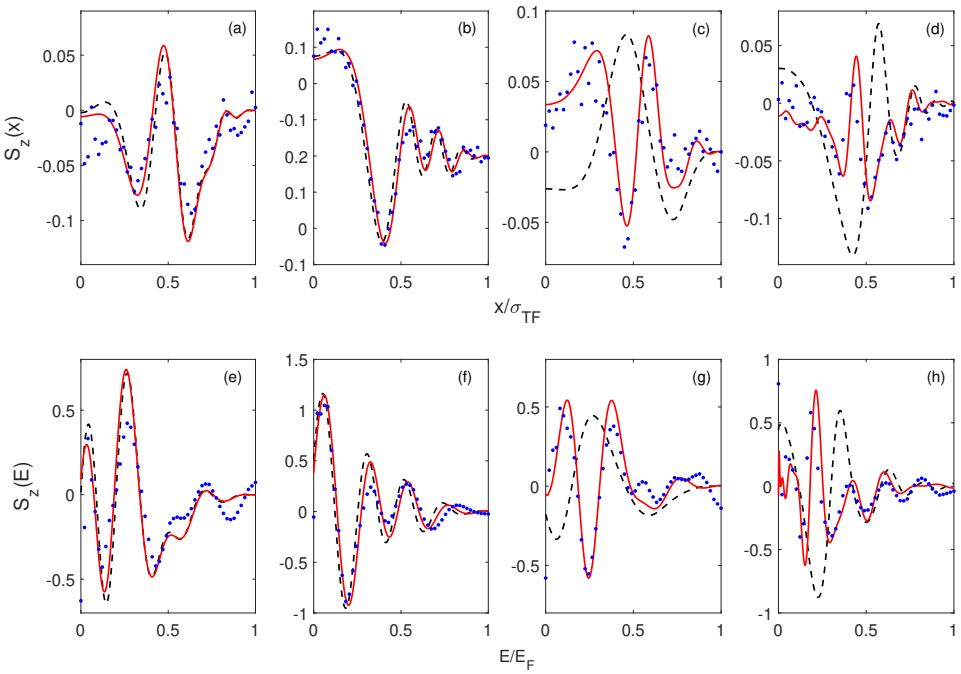

FIG. 4. Single-shot spin-density profiles in space (top) and in energy space (bottom) for perturbed quantum rewinding. For this set of data, $\sigma_{TF} \approx 340\,\mu$m, (a,e) measured scattering length $a = 5.2\,a_0$, $\phi_x = \pi/2$, $\tau = 200$ ms; (b,f) $a = 5.2\,a_0$, $\phi_x = \pi$, $\tau = 200$ ms; (c,g) $a = 8.0\,a_0$, $\phi_x = 3\pi/2$, $\tau = 200$ ms; (d,h); $a = 5.2\,a_0$, $\phi_x = \pi/2$, $\tau = 400$ ms. Blue dots are single-shot data. Red curves: Quasi-classical collective spin vector model using the measured scattering length, with forward and backward evolution phases φ_f and φ_b as fit parameters. Black-dashed curves show the fits using the analysis method of Ref. [20], which requires $a_{fit} = 9.0\,a_0$ for (a,e) and (b,f). Black dashed curves in (c,g) and (d,h) show typical fit failures for the same method.

the single-shot data (blue dots). For the model reported in this work, the forward and backward evolution phases φ_f and φ_b are treated as two free parameters. This model (red curves) is in good agreement with data taken with all experimental parameters ϕ_x and $[a;\,\tau]$ in Fig. 4: $[5.2\,a_0;$ 200 ms] data is shown in (a,e) and (b,f), $[8.0\,a_0;$ 200 ms] in (c,g) and $[5.2\,a_0;$ 400 ms] in (d,h). Additional data obtained at $[5.2\,a_0;$ 200 ms] with ϕ_x in steps of $\phi_x = \pi/4$ are shown in the supplement [21], demonstrating equally good agreement. Section IV B of the supplement explains the sources of minor defects observed in data for $[8.0\,a_0;$ 200 ms] and $[5.2\,a_0;$ 400 ms].

The model adopted in Ref. [20] assumes $\varphi_f \equiv \varphi_b + \pi$ mod 2π. The fits (black-dashed curves) to the data in Fig. 4 (a,e) and (b,f) for $[5.2\,a_0;$ 200 ms] require a *fitted* scattering length of $a_{fit} = 9.0\,a_0$ in disagreement with the measured value. The magnetic field calibration allows a precision of 0.03 a_0 in scattering length measurement, thus, this fitting parameter a_{fit} is unphysical. Therefore, Ref. [20] suggested a major breakdown of this quasi-classical model. In addition, this model fails to fit data in experiments implemented with parameters $[5.2\,a_0;$ 400 ms] and $[8.0\,a_0;$ 200 ms] regardless of the a_{fit} value. Black dashed curves in Fig. 4 (c,g) and (d,h) show typical fit failures of the Ref. [20] model. By analyzing single-shot data and including RF detunings correctly in the model, the experiment reported in this work validates the classical treatment of this large spin lattice undergoing perturbed quantum rewinding.

The modified model reported here explicitly shows the difficulty of multi-shot averaged measurements of transverse spin components, such as s_x, where the averages of $\cos\varphi_{fb}$ and $\sin\varphi_{fb}$ in Eq. 2 tend to vanish. Previously, the imperfect phase control problem was partially circumvented by using a maximum likelihood estimation [12]. However, Eq. 2, which is valid for both quasi-classical and full quantum treatments [21], suggests that multi-shot averaged measurements of energy-space spin operator products, such as $\langle s_{zi}s_{zj}\rangle = \langle \tilde{s}'_{xi}\tilde{s}'_{xj}\rangle$, are important, since the random-phase averages $\langle\cos^2\varphi_{fb}\rangle = \langle\sin^2\varphi_{fb}\rangle = 1/2$. This method enables improved out-of-time-order correlation measurements in quantum gases, where the W operator is unchanged and the operator $V = s_{xi}$ is replaced with $V = s_{xi}s_{xj}$, since the initial x-polarized state is an eigenstate of both operators [14, 20, 23].

In summary, this work verifies that a quasi-classical spin vector model of weakly interacting Fermi gases explains perturbed quantum rewinding experiments, using measurements of single-shot spin density profiles with sufficient resolution to enable quantitative study. The analysis reported here elucidates the effects of uncontrolled forward and backward evolution phases, φ_f and

φ_b, on the system and measurements, resolving an outstanding conflict with a previous treatment [20]. Our results suggest new correlation analysis methods based on energy-resolved operator products, which yield signals that are independent of the uncontrolled RF detuning without assuming phase distributions [12]. Applying such methods to measure the time dependence of correlations between transverse components $\langle \tilde{s}_{\perp i} \cdot \tilde{s}_{\perp j} \rangle$ allows the study of entanglement development in a large system [24] and investigations of many-body dynamics and information propagation[25]. Such experiments will be a topic of future work.

Primary support for this research is provided by the Air Force Office of Scientific Research (FA9550-22-1-0329). Additional support is provided by the National Science Foundation (PHY-2006234 and PHY-2307107).

*Corresponding authors: jhuang39@ncsu.edu
jethoma7@ncsu.edu

[1] R. Lewis-Swan, A. Safavi-Naini, J. Bollinger, and et al., Unifying scrambling, thermalization and entanglement through measurement of fidelity out-of-time-order correlators in the Dicke model, Nature Communication **10**, 1581 (2019).
[2] J. Eisert, M. Friesdorf, and C. Gogolin, Quantum many-body systems out of equilibrium, Nature Physics **11**, 124–130 (2015).
[3] A. M. Kaufman and et al., Quantum thermalization through entanglement in an isolated many-body system, Science **353**, 794 (2016).
[4] A. Auerbach, *Interacting electrons and quantum magnetism* (Springer-Verlag, New York, 1994).
[5] X. Du, L. Luo, B. Clancy, and J. E. Thomas, Observation of anomalous spin segregation in a trapped Fermi gas, Phys. Rev. Lett. **101**, 150401 (2008).
[6] X. Du, Y. Zhang, J. Petricka, and J. E. Thomas, Controlling spin current in a trapped Fermi gas, Phys. Rev. Lett. **103**, 010401 (2009).
[7] U. Ebling, A. Eckardt, and M. Lewenstein, Spin segregation via dynamically induced long-range interactions in a system of ultracold fermions, Phys. Rev. A **84**, 063607 (2011).
[8] S. Pegahan, J. Kangara, I. Arakelyan, and J. E. Thomas, Spin-energy correlation in degenerate weakly interacting Fermi gases, Phys. Rev. A **99**, 063620 (2019).
[9] F. Piéchon, J. N. Fuchs, and F. Laloë, Cumulative identical spin rotation effects in collisionless trapped atomic gases, Phys. Rev. Lett. **102**, 215301 (2009).
[10] S. S. Natu and E. J. Mueller, Anomalous spin segregation in a weakly interacting two-component Fermi gas, Phys. Rev. A **79**, 051601 (2009).
[11] C. Deutsch, F. Ramirez-Martinez, C. Lacroûte, F. Reinhard, T. Schneider, J. N. Fuchs, F. Piéchon, F. Laloë, J. Reichel, and P. Rosenbusch, Spin self-rephasing and very long coherence times in a trapped atomic ensemble, Phys. Rev. Lett. **105**, 020401 (2010).
[12] S. Smale, P. He, B. A. Olsen, K. G. Jackson, H. Sharum, S. Trotzky, J. Marino, A. M. Rey, and J. H. Thywissen, Observation of a transition between dynamical phases in a quantum degenerate Fermi gas, Science Advances **5** (2019), elocation-id: eaax1568.
[13] A. P. Koller, M. L. Wall, J. Mundinger, and A. M. Rey, Dynamics of interacting fermions in spin-dependent potentials, Phys. Rev. Lett. **117**, 195302 (2016).
[14] M. Gärttner, J. G. Bohnet, A. Safavi-Naini, M. L. Wall, J. J. Bollinger, and A. M. Rey, Measuring out-of-time-order correlations and multiple quantum spectra in a trapped-ion quantum magnet, Nature Physics **13**, 781 (2017).
[15] P. Ball, Evolution of spins looks surprisingly classical, Physics World **34(10)**, 6ii (2021).
[16] M. Lakshmanan, T. W. Ruijgrok, and C. J. Thompson, On the dynamics of a continuum spin system, Physica **84A**, 577 (1976).
[17] D. A.Garanin, K. Kladko, and P. Fulde, Quasiclassical Hamiltonians for large-spin systems, Eur. Phys. J. B **14**, 293 (2000).
[18] A. Das, M. Kulkarni, H. Spohn, and A. Dhar, Kardar-Parisi-Zhang scaling for an integrable lattice Landau-Lifshitz spin chain, Phys. Rev. E **100**, 042116 (2019).
[19] D. Schubert, J. Richter, F. Jin, K. Michielsen, H. De Raedt, and R. Steinigeweg, Quantum versus classical dynamics in spin models: Chains, ladders, and square lattices, Phys. Rev. B **104**, 054415 (2021).
[20] S. Pegahan, I. Arakelyan, and J. E. Thomas, Energy-resolved information scrambling in energy-space lattices, Phys. Rev. Lett. **126**, 070601 (2021).
[21] See the Supplemental Material for a description of the experimental details and of the quasi-classical spin model.
[22] G. Pretzier, A new method for numerical Abel-inversion, Zeitschrift für Naturforschung A **46**, 639 (1991).
[23] M. Gärttner, P. Hauke, and A. M. Rey, Relating out-of-time-order correlations to entanglement via multiple-quantum coherences, Phys. Rev. Lett. **120**, 040402 (2018).
[24] P. Jurcevic, B. Lanyon, P. Hauke, and et al., Quasiparticle engineering and entanglement propagation in a quantum many-body system, Nature **511**, 202 (2014).
[25] P. Hauke and L. Tagliacozzo, Spread of correlations in long-range interacting quantum systems, Phys. Rev. Lett. **111**, 207202 (2013).